Improving the seismic capacity of steel–concrete composite frames with spiral-confined slabs

Marco Fasan[1], Chiara Bedon[1] ⓘ, Nicola Troiano[1] and Claudio Amadio[1]

Abstract

The seismic performance analysis of steel–concrete composite frames involves, as known, the interaction of several load-bearing components that should be properly designed, with multiple geometrical and mechanical parameters to account. Practical recommendations are given by the Eurocode 8 (EC8) – Annex C for the optimal detailing of transverse rebars, so as to ensure the activation of conventional resisting mechanisms. In this paper, the attention is focused on the analysis of effects and benefits due to a novel confinement solution for the reinforced concrete (RC) slab. The intervention is based on the use of diagonal steel spirals, that are expected to enforce the overall compressive response of the RC slab, thanks to the activation of an optimized strut-and-tie resisting mechanism. The final expectation is to first increase the resistance capacity of the slab that can thus transfer higher compressive actions under seismic loads. Further, as shown, the same resisting mechanism can be beneficial for the yielding of steel rebars, depending on the final detailing of components, and thus possibly improve the ductility of the system. To this aim, a refined finite element (FE) numerical analysis is carried out for several configurations of technical interest. The in-plane compressive behaviour and the activation of resisting mechanisms are explored for several spiral-confined slabs, based on various arrangements. Major advantage is taken from literature experimental data on RC slabs that are further investigated by introducing the examined confinement technique. The attention is hence given to the local and the global structural effects due to different arrangements for the proposed steel spirals. As shown, once the spirals are optimally placed into the slab, the strength and ductility parameters of the concrete struts can be efficiently improved, with marked benefits for the overall resisting mechanisms of the slab, and thus for the steel–composite frames as a whole.

Keywords

steel–concrete composite frames, spiral reinforcement, slab confinement, finite element numerical analysis

Introduction

The use of continuous spiral reinforcements can be an efficient solution for the seismic performance improvement of reinforced concrete (RC) members, due to their positive confinement effects. Several literature studies prove their potential especially for concrete columns, where both the ductility and energy dissipation capacity can be greatly improved. Positive applications can be found, for example, in Marvel et al. (2014) and Sankholkar et al. (2018), based on glass fibre–reinforced polymer (GFRP) or steel spirals, respectively. In Simões et al. (2001) and Simões and Simões da Silva (2001), the attention has been paid on the identification of concrete confinement contribution on composite columns belonging to steel–concrete composite frames, as well as on the assessment of strength and stiffness degradation.

The analysis and design of steel–concrete composite frames, in this regard, is a challenging issue that requires multiple attentions, due to a combination of multiple geometrical and mechanical parameters that should be satisfied to optimize the expected seismic performances. To this aim, a number of experimental, analytical and numerical investigations have been dedicated to the assessment of resisting mechanisms and to the definition of design proposals (Aribert et al., 2006; Li et al., 2011; Pecce and Rossi, 2015; Salvatore et al., 2005; Thermou et al., 2004; Tartaglia et al., 2018), in support or refinement of conventional approaches that can be found in the Eurocode

[1]Department of Engineering and Architecture, University of Trieste, Trieste, Italy

8 (EC8) for seismic resistant steel–concrete composite frames (CEN, 2004).

In this paper, the attention is focused on the use of steel spirals for the seismic reinforcement of slabs belonging to composite steel–concrete frames. The goal is to assess and optimize the spiral-based confinement effect and its benefits to improve the role of the slab on the overall joint response in seismic conditions.

In doing so, a special attention is spent for the finite element (FE) numerical analysis of several configurations of technical interest (Simulia, 2020), with a focus on both the local and the global structural effects due to different design and/or arrangement of spirals specifically introduced into the slab to improve the strength and ductility of concrete struts for the composite joint. To this aim, Section Problem definition and design proposal introduces the basic assumptions and design methods of steel–concrete composite systems, according to EC8 – Annex C provisions for seismic design. The implementation of the proposed technique, as shown, finds place in internal joints under seismic combinations of loads. In the Section Slab confinement with steel spirals, the spiral-based confinement technique is described, while the Sections Numerical analysis of a spiral-confined RC slab and Discussion of results present practical applications to a slab prototype in compression that is adapted from past literature studies. In the Section Analysis of a full-scale steel–concrete composite frame, finally, the same technique is applied to a full-scale RC slab belonging to a real steel–concrete composite frame (internal joint). Major advantage for the analysis of load-bearing capacities and failure mechanisms is taken from the FE numerical analysis of RC slabs under in-plane compression.

As shown, the detailing of spirals is crucial to ensure the activation of optimized resisting mechanisms. Besides, once the spirals are properly arranged in the slab, the overall compressive resistance of the slab can be largely increased, with enhanced benefits for the steel–concrete composite frames. Further, the introduction of steel spirals can also improve the whole post-cracked stage of the steel–concrete composite system, given that (depending on the desired yielding of transverse reinforcement in the slab) even major ductility in the slab can be achieved.

Problem definition and design proposal

Resisting mechanisms

The optimal design of steel–concrete composite frames is a complex issue that involves a multitude of parameters. The transverse reinforcement has a key role for the global resistance of composite joints, but is also responsible of the angle and length of spreading of compressive stresses in concrete. The amount and position of transverse rebars should be optimally designed to ensure the formation of compression struts in contact with the column, and to transfer the composite action from the RC slab to the column. At the same time, the optimal detailing of rebars can allow to guide the overall mechanical behaviour of the composite structure towards a ductile mechanism (due to yielding of rebars), in place of a brittle failure mechanism (due to crushing of concrete), and thus allowing a greater absorption of energy under seismic events.

Figure 1 schematizes the typical activation of resisting mechanisms for slabs in compression. Besides the presence of struts strictly depends on the nodal configuration, the design of transverse steel rebars (A_T) is based on the so-called 'mechanism 1' (direct compression on the column flange) and 'mechanism 2' (compressed concrete struts inclined to the column sides).

Further, for the purpose of the present study, the possible activation of 'mechanism 3' (which is related to crushing of concrete due to contact with shear studs of the transverse beam) is disregarded (Amadio et al., 2016).

The maximum compressive force transmitted to the column through each mechanism can be estimated in EC8 – Annex C as

$$F_{Rd,1} = b_b d_{eff} \left(\frac{0.85 f_{ck}}{\gamma_c} \right) \tag{1}$$

$$F_{Rd,2} = 0.7 h_c d_{eff} \left(\frac{0.85 f_{ck}}{\gamma_c} \right) \tag{2}$$

where b_b is the bearing width of the concrete slab in contact with the column, d_{eff} the overall depth of the slab (in case of solid slabs) or the thickness of the slab above the ribs of profiled sheeting (for composite slabs), h_c the height of the column, f_{ck} the characteristic compressive strength of concrete and γ_c the concrete partial safety factor.

Following EC8 recommendations, the required A_T must be quantified so as to allow the complete crushing of struts. This corresponds to a maximum force transmitted by the RC slab equal to

$$F_{c,slab,Rd} = F_{Rd,1} + F_{Rd,2} \tag{3}$$

From equation (1), it follows that the minimum amount A_T able to satisfy the translational equilibrium of the system is given by

$$A_{T,1} \geq \frac{F_{t,1}}{f_{yk}/\gamma_s} = \frac{F_{Rd,1}}{2\left(f_{yk}/\gamma_s\right)} \tan\alpha = \frac{F_{Rd,1}}{4\left(f_{yk}/\gamma_s\right)} \frac{\left(b_{eff}^+ - b_b\right)}{b_{eff}^+}$$
$$= \frac{F_{Rd,1}}{4\left(f_{yk}/\gamma_s\right)} \frac{0.15l - b_b}{0.15l} \tag{4}$$
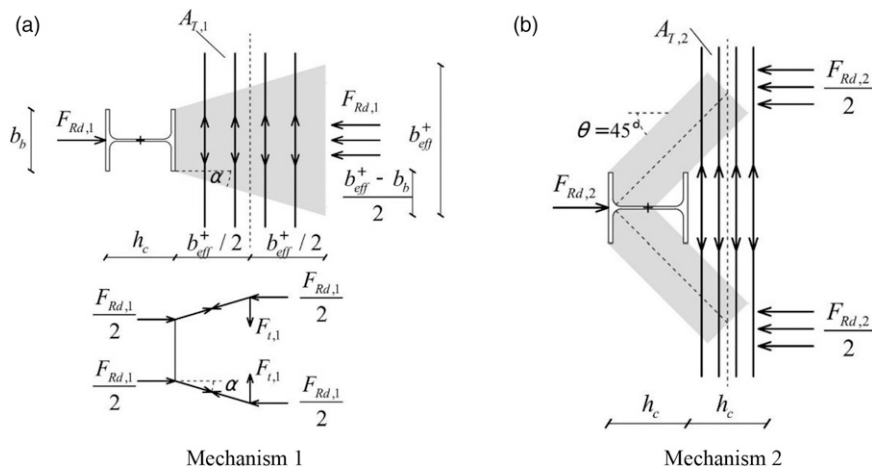
Figure 1. Conventional strut-and-tie resisting mechanisms for concrete slabs, according to EC8 – Annex C provisions. (a) Mechanism 1, (b) Mechanism 2.
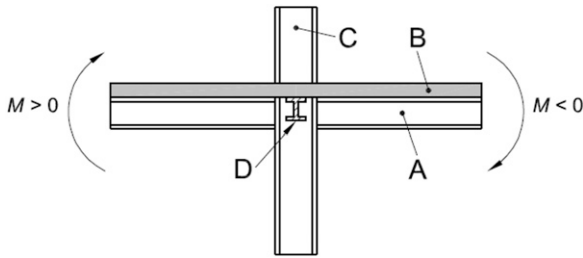

Figure 2. Steel–concrete composite frame (internal joint) in seismic conditions, as for EC8 – Annex C.

$$A_{T,2} \geq \frac{F_{Rd,2}}{2\left(f_{yk}/\gamma_s\right)} \qquad (5)$$

where f_{yk} is the characteristic yielding strength for steel; γ_s, the corresponding partial safety factor, α, the angle of spreading of the compressive stresses, b_{eff}^+, the seismic effective width of the beam under sagging moment ($M > 0$); and l, the length of the beam.

Axial forces in the slab

For steel–concrete composite frames, the transmission of axial forces from the RC slab to the column represents a critical aspect for design. On one side, the detailed design of steel rebars as in the Section Resisting mechanisms can support the activation of resisting mechanisms that agree with EC8 strategies. On the other side, and especially for internal composite joints, these mechanisms are required to equilibrate the internal axial forces on both sides of the column. This means that especially under a seismic combination of loads as in Figure 2, the required axial force to transfer to the RC slab is the sum of two components.

From a practical point of view, more in detail, the EC8 requires that

$$1,2\left(F_{sc} + F_{st}\right) \leq \sum_i F_{Rd,i} \qquad (6)$$

where $F_{sc} = b_{eff}^+ d_{eff} f_{cd}$ is the compressive term due to $M > 0$ and $F_{st} = A_s f_{sd}$ is the tensile term deriving from $M < 0$. To satisfy equation (6), three options are available, namely: (a) increase of d_{eff}; (b) activation of the so-called 'mechanism 3', or (c) increase of f_{cd} based on confinement.

Slab confinement with steel spirals

In the present study, a new confinement technique based on the use of steel spirals is assessed for the seismic improvement of RC slabs in steel–concrete composite frames. More in detail, the proposed spirals are expected to improve the overall compressive capacity of the slab, and thus positively affect the overall resisting 'mechanism 2' earlier summarized in the Section Problem definition and design proposal. The concept takes advantage of the strut-and-tie configuration and can be qualitatively schematized as in Figure 3.

From a mechanical point of view, the intervention is based on the use of circular steel spirals that can be placed as in Figure 4a, and involves the use of a number of circular members as in Figure 4b. Worth to be noted that the proposed solution can take equivalent benefit from the use of rectangular stirrups as in Figure 3.

The expected confinement effects is directly proportional to the amount of steel and the confined volume of concrete, given that the lateral confinement pressure is

$$\sigma_l \propto \frac{A_{st}}{s A_{conf}} \qquad (7)$$

with A_{st}, A_{conf} the resisting section of steel and confined concrete, s the pace of spirals. Further, equation (7) can be
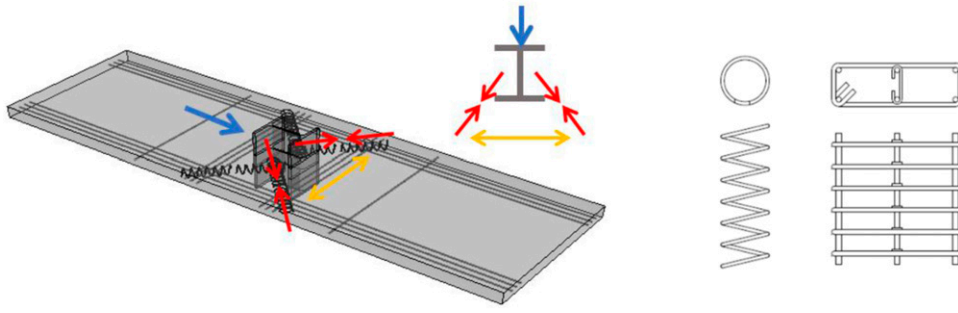
Figure 3. Qualitative axonometric view of spiral-based confinement mechanism, with detail view of circular spirals or equivalent rectangular stirrups.

adapted for groups of spirals (with geometrical parameters that are defined according to Figure 4b), where

$$\sigma_l = \sqrt{\frac{n_x n_y}{b_x b_y}} \frac{A_{st} f_{sk}}{s} \tag{8}$$

The overall confinement technique finds application in the mechanical model of the traditional joint schematized in Figure 5. The response of un-confined RC slabs in compression can be characterized by a total stiffness contribution that is given by the sum of stiffness terms from the mechanisms '1' and '2', respectively (Amadio et al., 2016)

$$k_c = k_{c,1} + k_{c,2} \tag{9}$$

Following Figure 5, with 's' and 't' denoting the strut-and-tie contributions, respectively, both the terms $k_{c,1}$ and $k_{c,2}$ can be expressed from simple geometrical considerations under small-displacement assumptions. The analysis of the slab in compression and the corresponding axial displacements u under an imposed axial force F can be in fact helpful to express

$$u = [u_t + u_s \text{sen}(\theta + \theta)]\text{tg}(\theta + \theta/2) + u_s \cos(\theta + \theta) \tag{10a}$$

For small-displacement assumptions and small angular variations, equation (10a) gives the compact expression

$$u = u_s \sec\theta + u_t \text{tg}\theta \tag{10b}$$

The equilibrium in Figure 5 can be described in the form of elastic forces, given that $F_s = 0.5F/\cos\theta$ in each strut and $F_t = 0.5F\text{tg}\theta$ in the tie. The hypothesis of linear elastic behaviour for each component, under a total axial force $F = Ku$ for the mechanism (with $K = E_a k$), corresponds to

$$\begin{cases} F_s = K_s u_s & => & K_s = E_a k_s \\ F_t = K_t u_t & => & K_t = E_a k_t \end{cases} \tag{11}$$

Consequently, the combination of equations (10b) and (11) leads to

$$\frac{1}{k} = \frac{1 + \text{tg}^2\theta}{k_s} + \frac{\text{tg}^2\theta}{k_t} \tag{12}$$

Finally, given that $\text{tg}\theta = l_y/l_x$ (with l_x, l_y defined as in Figure 4a, the equilibrium of the system in Figure 5 suggests that

$$k_{c,1} = \frac{1}{\frac{1+\text{tg}^2\theta}{k_s} + \frac{\text{tg}^2\theta}{k_t}} \tag{13a}$$

$$k_{c,2} = \frac{2}{\frac{1+\left(\frac{l_y}{l_x}\right)^2}{k_s} + \frac{\left(\frac{l_y}{l_x}\right)^2}{k_t}} = \frac{2}{\frac{2}{k_s} + \frac{1}{k_t}} \tag{13b}$$

with

$$k_s = d_{eff} \frac{1 - \text{tg}^2\theta}{1 + \text{tg}^2\theta} \frac{E_{cm}}{E_a} \tag{14}$$

$$k_t = \frac{4A_{T,1}}{b_{eff}^+} \tag{15}$$

Following the above geometrical and mechanical considerations about resistance and stiffness properties, the current research study aims at further improving the strut-and-tie resisting mechanism by placing steel spirals in the region of struts. Once these spirals are properly arranged to activate the interaction of the column with the transverse rebars, as shown, the slab as a whole can take maximum benefits.

Numerical analysis of a spiral-confined RC slab

Setup and confinement

The reference specimen was derived from the experimental investigation originally presented in Braconi et al. (2007). The layout agreed with Figure 6 and consisted of a segment of steel column (HEB280) with a trapezoidal RC slab (100 mm in thickness, f_{ck} = 35 MPa). A set of 5 ϕ 12
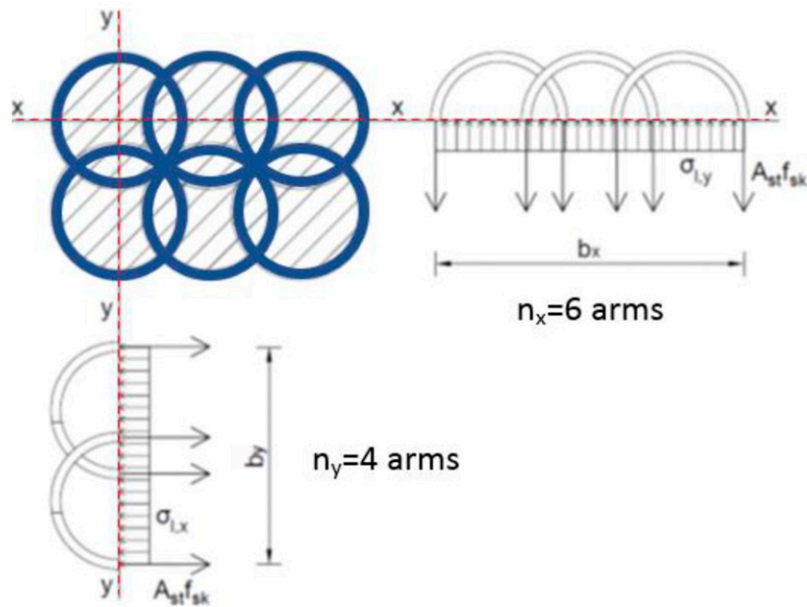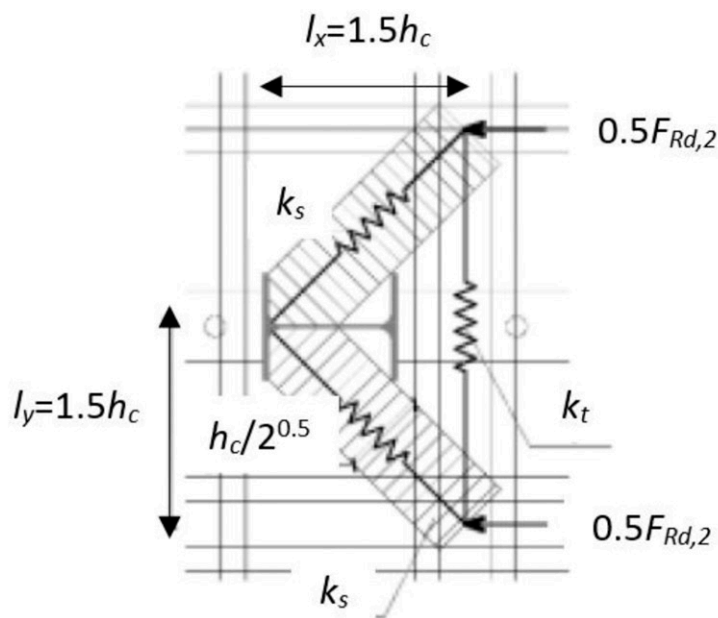
Figure 4. Schematic equilibrium for the confinement effect of spirals group: (a) activation of the resistant mechanism, and (b) detail of geometrical parameters (example).

tension bars and a 150 × 150 mm, φ 8 mesh were also used for concrete reinforcement (f_y = 390 MPa). In addition, 4 φ 8 stirrups were placed in the column region. Finally, a 40 mm thick opening was placed in front of the column stub, for the de-activation of the resistant 'mechanism 1' as in EC8. The boundary conditions of the slab specimen were realized in the form of two simple supports (280 mm in width for each support). The extension of the supports, as well as the 45° inclination for the upper part of the slab, was derived from the original design in Braconi et al. (2007), in

order to force the complete development of resistant 'mechanism 2'. The vertical compressive load was in fact imposed in Braconi et al. (2007) to the top face of the steel column, while monitoring the relative vertical deformation of the slab.

In presence of 'mechanisms 2' only, like for the slab in Figure 6 (where a frontal opening to the steel column flange was made), the EC8 requires that the cross-section of the transverse rebars should be calculated as in equation (5). For the purpose of the present study, the reference slab
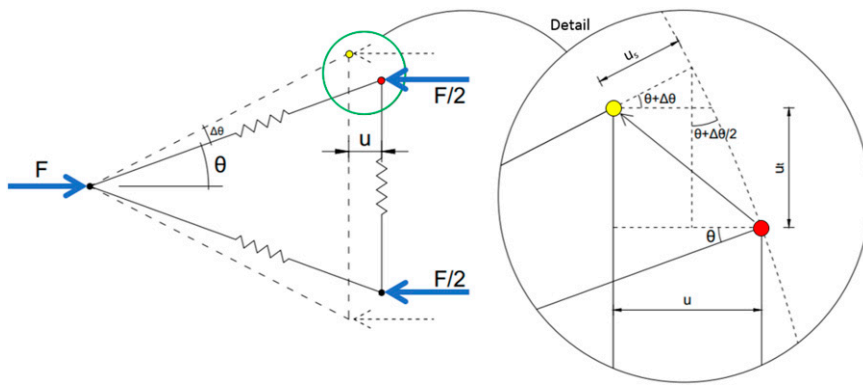
Figure 5. Reference mechanical model for the definition of stiffness contributions of the strut-and-tie resisting mechanism for the RC slab in compression.
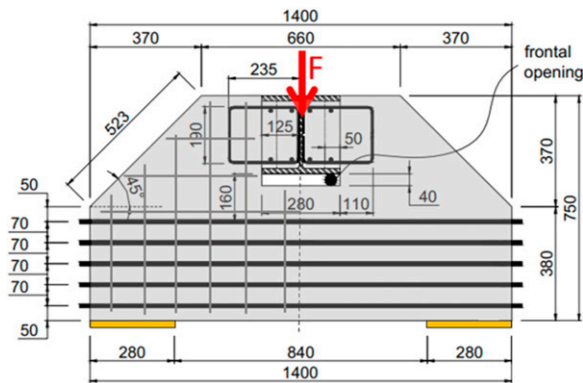

Figure 6. Unreinforced slab specimen for the compressive performance assessment: in evidence, the nominal geometry (dimensions in mm) and the test setup (front view). Setup adapted from Braconi et al. (2007).

configuration was preliminarily derived from the nominal geometry of Figure 6. The developed FE numerical models were thus validated to the geometrical and mechanical properties discussed in Braconi et al. (2007), and then adapted to the current investigation with additional spirals.

The typical confinement technique took the form of Figure 7, in which the additional spirals are highlighted in red colour. Further, through the numerical parametric investigation, various configurations (in terms of number, inclination) were taken into account for the introduction of the spirals, so as to optimally connect the column/load introduction region with the bottom transverse rebars. The expected working mechanism under the effects of the imposed compressive force F is also emphasized in Figure 7.

Finite element numerical modelling

The numerical analysis was carried out in ABAQUS/Explicit, in the form of nonlinear dynamic simulations with a quasi-static deformation regime. The typical geometry in Figures 6 and 7

was reproduced in the form of solid brick elements, while mono-dimensional B31 type beam elements were used for the steel tension bars and stirrups. The steel spirals for the confinement of the slab (circular type, 8 mm in nominal diameter) were also described with solid brick elements. Further, to avoid local damage effects at the symmetry plane, the full geometry was reproduced. Figure 8 shows the assembled FE model.

The overall modelling approach took inspiration from Amadio et al. (2017a, 2017b) in terms of geometrical and mechanical characterization of the involved load-bearing components, while the damage behaviour of concrete under axial compression was specifically calibrated in its input terms in accordance with Alfarah et al. (2017).

The 'embedded' constraint was used for all the steel reinforcing and confinement components (transverse rebars, reinforcement mesh, stirrups and spirals), that were assumed as rigidly bonded to the hosting RC slab. A rigid 'tie' constraint was used at the interface of the HEB280 profile and the corresponding surfaces of concrete. Any kind of possible relative sliding and rotation was thus disregarded. The same modelling approach was used for the steel supports at the base of the RC slab, that were rigidly bonded by 'tie' constraints for the involved surfaces of contact. Nodal restraints were thus defined at the base of steel supports and at the top face of the steel column (Figure 8a).

The vertical compressive load F was then introduced in the FE models in the form of a displacement-controlled setup, with a monotonic vertical displacement applied to the top surface of the HEB280 column. For the increasing vertical displacement, the vertical reaction forces at the base supports were continuously monitored, together with the relative vertical deformation of the RC slab. Similarly, the propagation of maximum stress and strain peaks in all the FE components was continuously monitored through the typical analysis. A special care was spent for the analysis of damage mechanism, including both the possible yielding of steel rebars but also the progressive fracture and cracking of the RC slab.
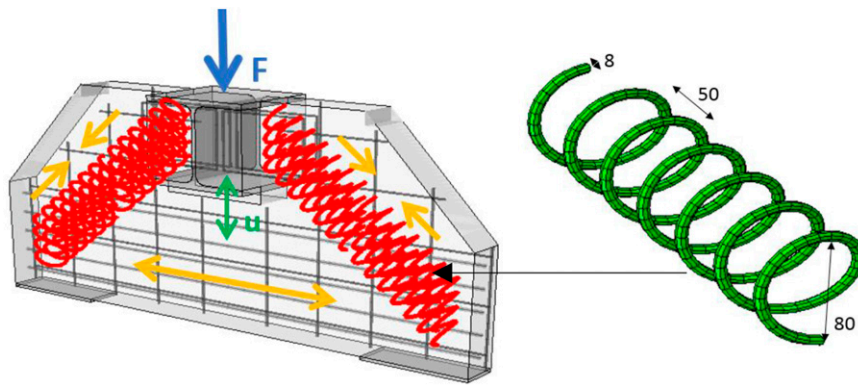
Figure 7. Expected resisting mechanism for the slab with additional steel spirals, and detail view of the circular spirals (dimensions in mm).
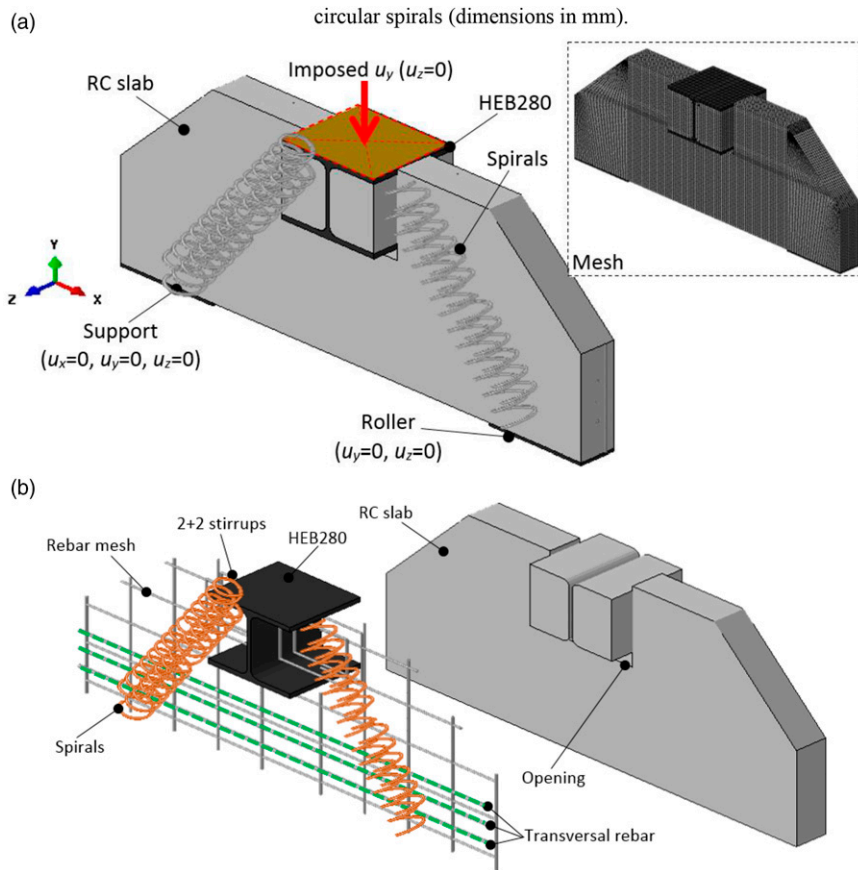

Figure 8. Numerical model of the RC slab confined with steel spirals (ABAQUS): (a) setup and mesh, (b) with evidence of components.

In order to ensure a realistic fracture pattern in the RC slab, a variable mesh pattern was in fact used for the discretization of solid brick elements. Based on a pre-liminary parametric study on the effect of mesh pattern, the final edge size was set in the range from 7 mm (especially in the region of expected fracture) to a maximum of 20 mm. The resulting discretization scheme can be seen in Figure 8a. This choice was suggested by the need to capture any local fracture in the slab, through the whole loading stage, as well as to monitor the evolution of stress distri-butions in the involved load-bearing components of the system. Most of the mesh pattern (≈90%) consisted of hexahedral solid elements, while a minimum part of wedge elements was used in the corner regions, so as to respect the
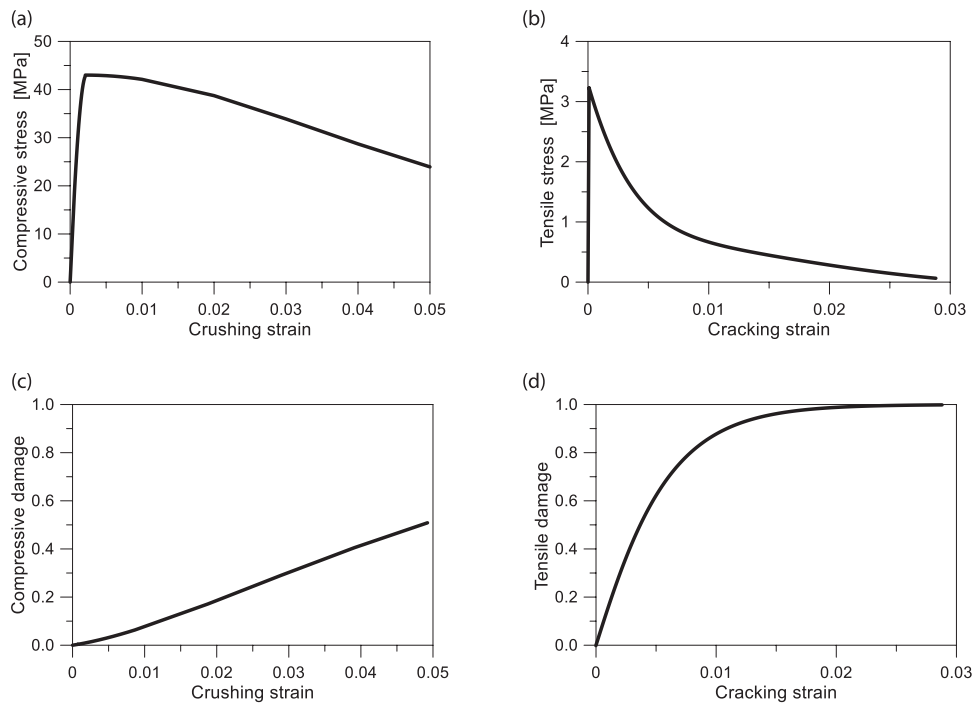
Figure 9. Input constitutive laws for the CDP material model (f_{ck} = 35 MPa), based on Alfarah et al. (2017): (a) compressive and (b) tensile behaviours, with (c)-(d) corresponding damage trends.

trapezoidal shape of the slab. The final pattern consisted in 130,000 elements and 420,000 DOFs.

A key role was assigned to material constitutive laws. While an equivalent elastic-plastic constitutive law was used for all the steel components, the 'Concrete Damaged Plasticity' (CDP) material model was taken into account for concrete. For all the constitutive laws in tension, compression or damage stage, nominal material properties are considered, based on the resistance classes defined in Braconi et al. (2007). Due to the imposed setup, differing from Amadio et al. (2017a, 2017b), the empirical constitutive laws proposed in Alfarah et al. (2017) and validated to uniaxial tests are taken into account. The additional advantage is that the formulation in Alfarah et al. (2017) still applies to the CDP model used in Amadio et al. (2017a, 2017b), but introduces a new set of parameters that allow to calibrate damage laws as a function of the mesh size l_{eq}. In this manner, severe premature degradation phenomena due to singular points in the setup of Figure 8 can be avoided. Figure 9 summarizes the input laws that were adopted in the current numerical investigation (f_{ck} = 35 MPa and l_{eq} = 7 mm for the current study).

Model validation to past experiments

The nonlinear dynamic analysis was hence performed in the form of a dynamic explicit loading stage, with a fictitious total step time of 600 s and a maximum imposed displacement of 5 mm. The above input parameters for material properties and

mesh pattern resulted in a mean automatic stable increment of 1.5×10^{-6} seconds. The analysis efficiency was properly enforced with the support of a 'fixed' mass-scaling technique. The quasi-static evolution of stress-strain phenomena was thus guaranteed by control of strain and kinetic energetic terms of the whole FE assembly. For the same reason, damping was disregarded through the analysis. Under the imposed setup and displacement, the typical FE analysis crashed at a total vertical deformation of ≈3.5–4 mm. The corresponding energy evolution is shown in Figure 10, where the mostly null kinetic term can be noticed through the step time.

An example of comparative FE results for the validation stage is also shown in Figure 11. The modelling strategy of the current study proved to offer very close correlation with literature experimental data. In Figure 11a, the numerical force-displacement response is compared to two different laboratory specimens discussed in Braconi et al. (2007). For the validation process only, the concrete properties are calculated with an actual f_{ck} = 33 MPa, as in the experiments from Braconi et al. (2007). The first damage initiation was found to appear at very small deformations, around 0.6 mm of imposed displacement. The stress peaks in transverse rebars approach the yield resistance at approximately 2 mm of imposed displacement (Figure 11b). Concrete cracks spread at around 30° from the column region Figure 11c), and the fracture evolution can be found in agreement with earlier experimental findings discussed in Braconi et al. (2007; box detail). The stress peaks in steel
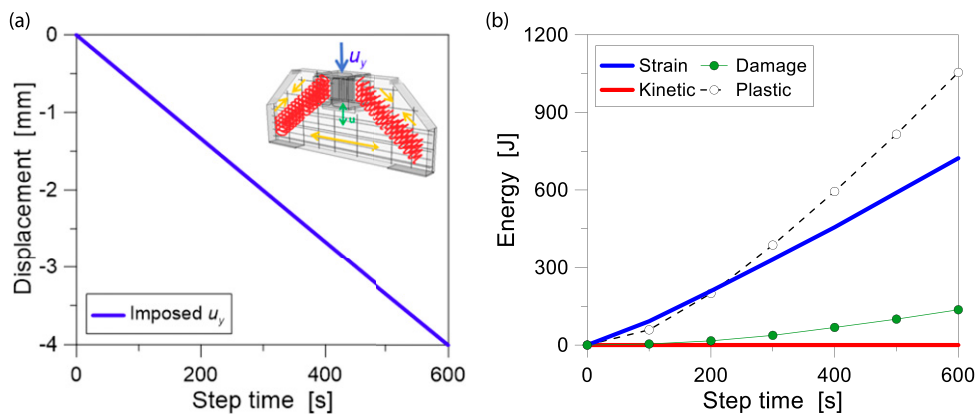
Figure 10. Numerical analysis of the RC slab (ABAQUS): (a) imposed vertical displacement and (b) example of corresponding energy terms, as a function of step time.
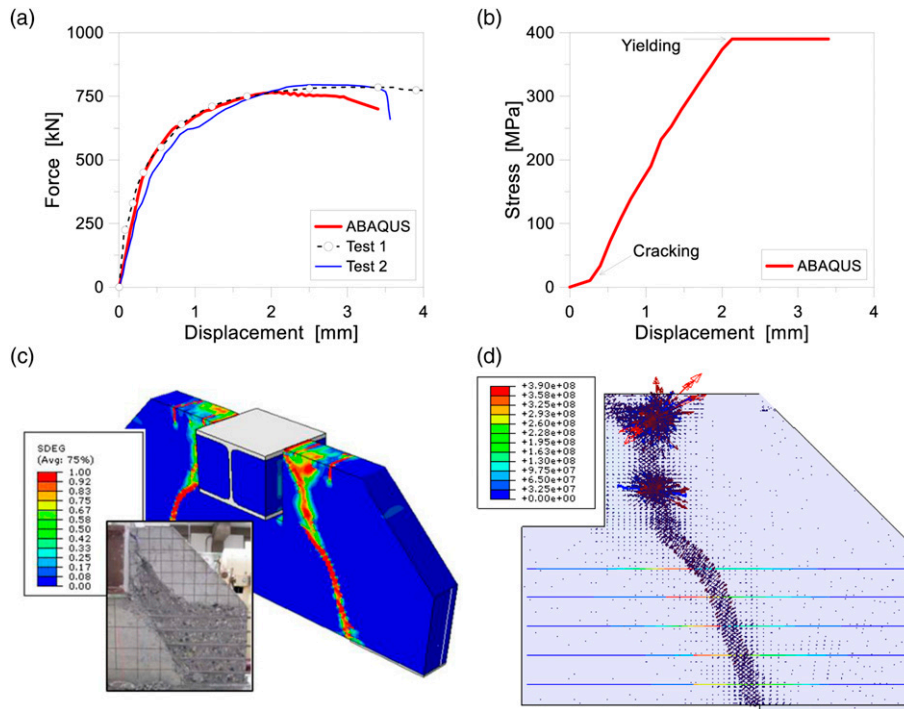

Figure 11. Numerical analysis of the RC slab (ABAQUS): (a) imposed vertical displacement and (b) example of corresponding energy terms, as a function of step time.

rebars, accordingly, are first reached at the interception of bars and concrete cracks (Figure 11d). This finding suggests that steel spirals should be arranged to capture the strut-and-tie mechanism of the composite system.

Discussion of results

Load-bearing capacity

At first, the analysis of parametric numerical results is carried out by comparison of the collected compressive load and vertical displacements for the selected configurations. Figure 12 shows some of the most relevant configurations for the numerical study discussed herein. The response of the unreinforced RC slab is plotted as a base reference for the analysis of local and global effects due to the proposed spirals.

In this regard, the presented comparisons are strictly related to the geometrical features of the laboratory prototype from Braconi et al. (2007), as well as to the resistance class of the involved materials. Besides, some useful trends can be still obtained for the validation of the spiral-confinement technique, towards the application to full-scale systems.
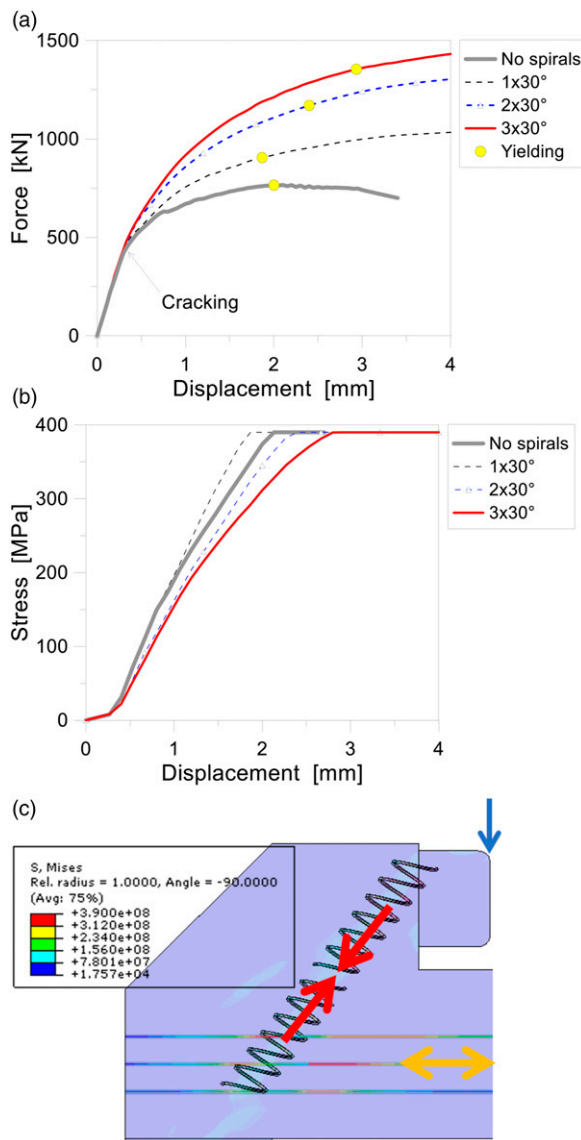
Figure 12. Analysis of the RC slab with various arrangements of steel spirals (ABAQUS): (a) load–displacement response and (b) stress in rebars (30 °) and (c) resisting mechanism (1 × 30 °, legend in Pa).

Figure 13. Load–displacement analysis of the RC slab with various arrangements of steel spirals (ABAQUS).

Moreover, Figure 12 gives evidence of the first cracking initiation of concrete and the first yielding for the transverse bars. For all the configurations, the crack propagation was observed to start propagating from the column flanges, and then to compromise the overall resistance and stiffness of the system. Anyway, the presence of steel spirals results in marked increase of global compressive capacity for the same slab. The initial elastic stiffness minimally increases with the number of steel spirals, and first cracks still initiate around 0.6 mm of imposed deformation. More interestingly, the post-cracked stiffness and resistance increase largely and are
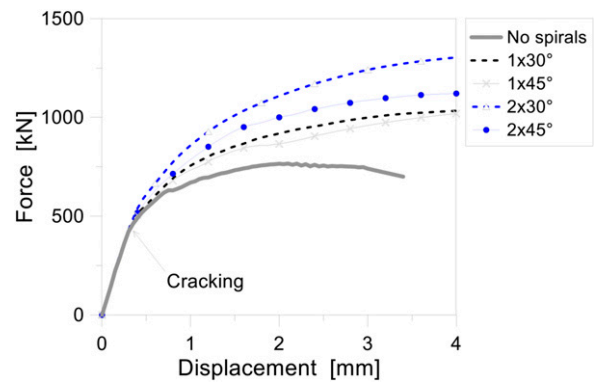
characterized by a more stable performance of the slab (Figure 12a). Moreover, the more the steel spirals are introduced, the more ductility can be achieved due to yielding of the tension rebars (Figure 12a), thus requiring an optimal design of all the mechanism components. Yellow dots in Figure 12b are representative of the first yielding for the transverse reinforcement of the slab, based on continuous monitoring of stress peaks for the resisting mechanism that is schematized in Figure 12c.

As far as the steel spirals are not properly arranged in terms of inclination for the desired strut-and-tie mechanism, the benefits can fully vanish and minimize the potential of the approach. An example is shown in Figure 13 for the same slab prototype. The solution with 1 × 45° spirals is still in close correlation with the 1 × 30° model. Otherwise, it is possible to see that the 2 spirals with 45° inclination roughly provide the same resistance increase of the 2 × 30° configuration.

Stress flow and damage evolution

The stress evolution and damage propagation/cracking in the concrete slab can be efficiently investigated in terms of vectorial stress patterns or evolution of the SDEG non-dimensional parameter (0 for uncracked concrete and 1 for fully damaged concrete, in accordance with the input parameters of Figure 9. Figure 14 presents the vectorial distribution of stress peaks and plastic strain, respectively, in the RC slab, at a vertical deformation of 1 mm, without or with 2 × 30° spirals. The comparison gives evidence of major damage for the un-confined slab, with benefits due to the steel spirals. For comparative purposes, Figure 15 presents also the fracture pattern (SDEG parameter) for the un-confined or confined slab with 2 × 30° spirals, at the same deformation stage.

In the first case, the propagation of cracks clearly affects the overall resistance and stiffness parameters of the slab in compression. Conversely, once the steel spirals (and rebars)
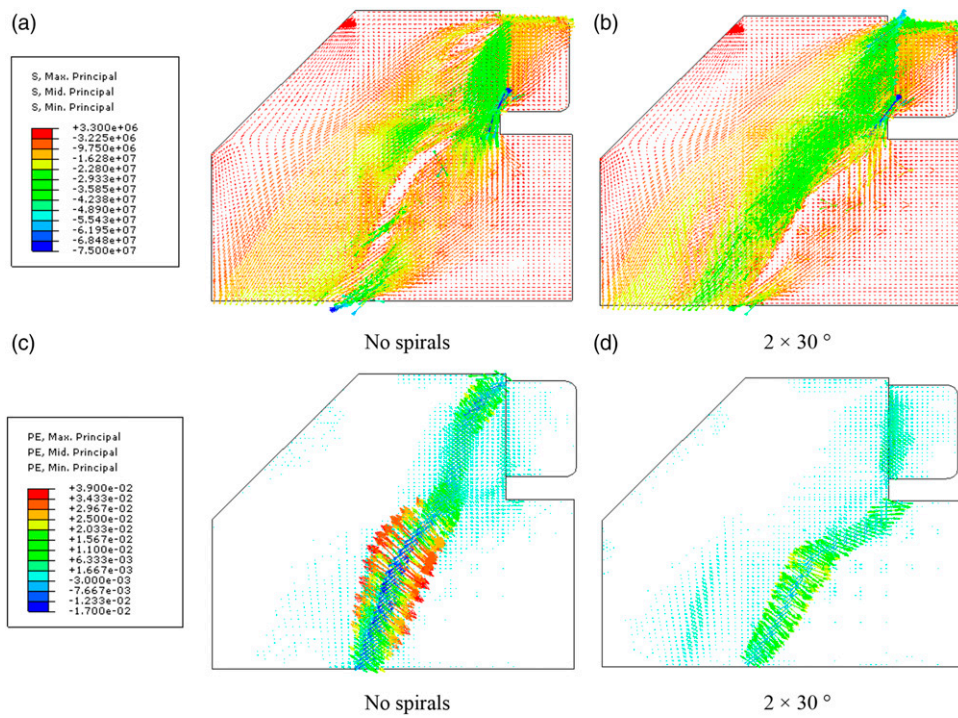
Figure 14. Vectorial distribution of (a)-(b) stress peaks and (c)-(d) plastic strain in the slab, as observed at 1 mm of vertical displacement (ABAQUS; in evidence, 1/2th nominal geometry).
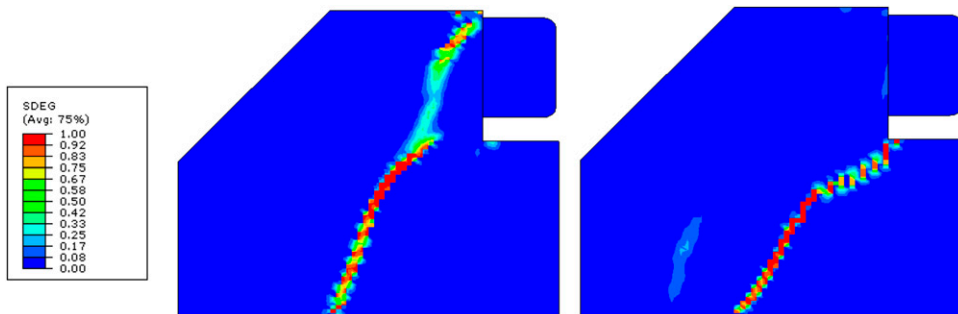

Figure 15. Damage (SDEG) for the slab (a) without or (b) with 2 × 30 ° steel spirals, as observed at 1mm of vertical displacement (ABAQUS; in evidence, 1/2th nominal geometry).
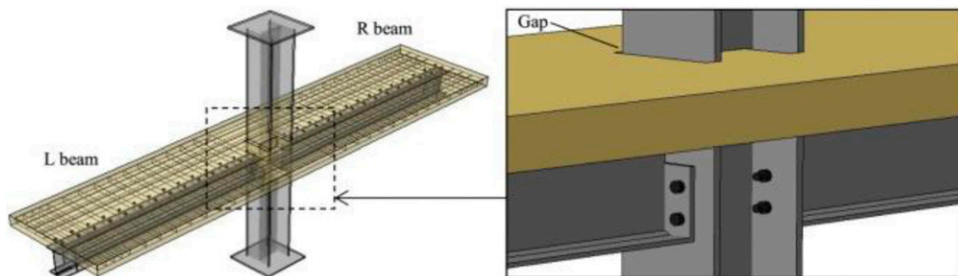

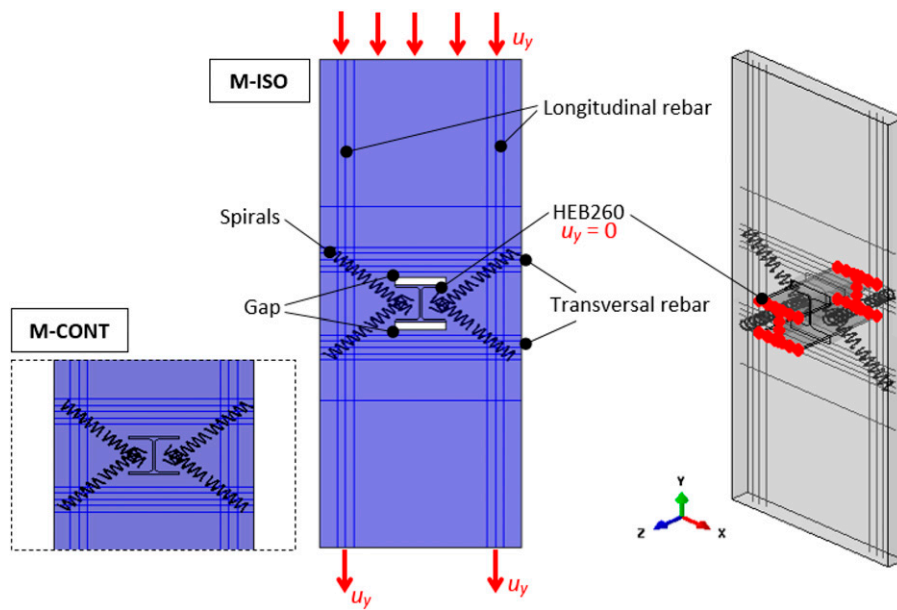**Figure 16.** Selected steel–concrete composite frame and joint detail.

Figure 17. Numerical setup for the analysis of confining steel spirals in full-scale slabs (ABAQUS).
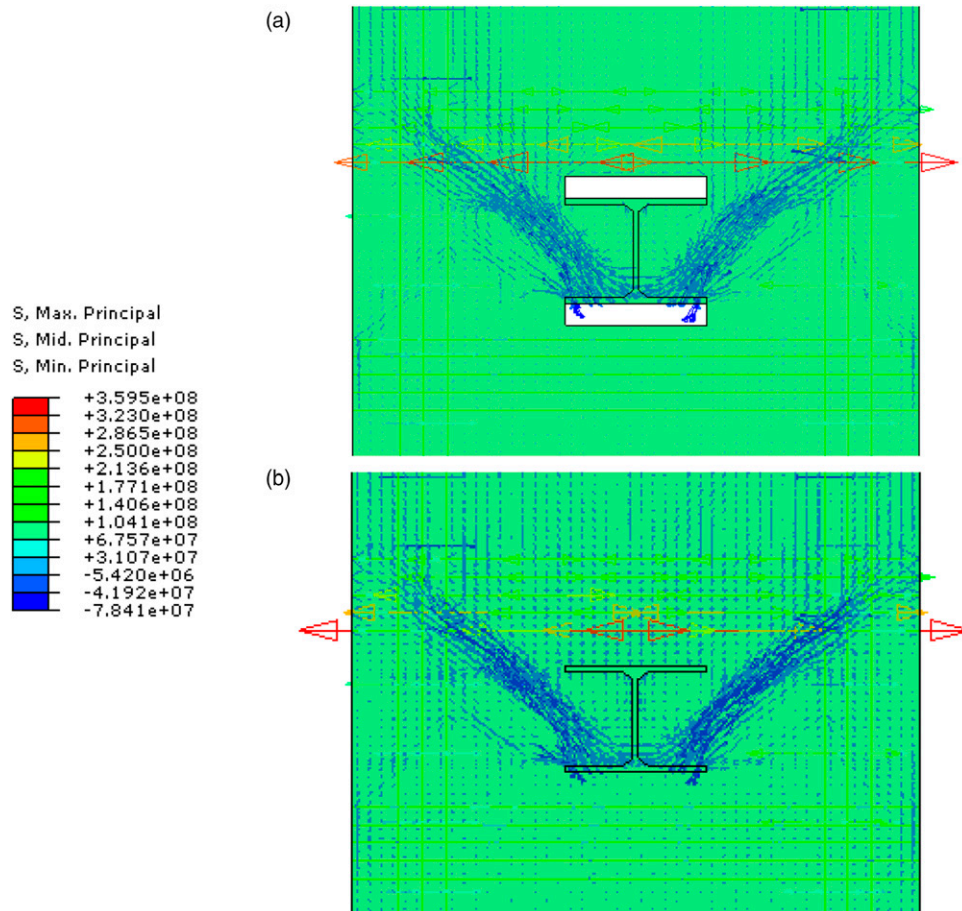

Figure 18. Qualitative stress distribution in the steel and concrete components due to spiral-confinement mechanism (ABAQUS): (a) M-ISO and (b) M-CONT. Legend values in Pa.
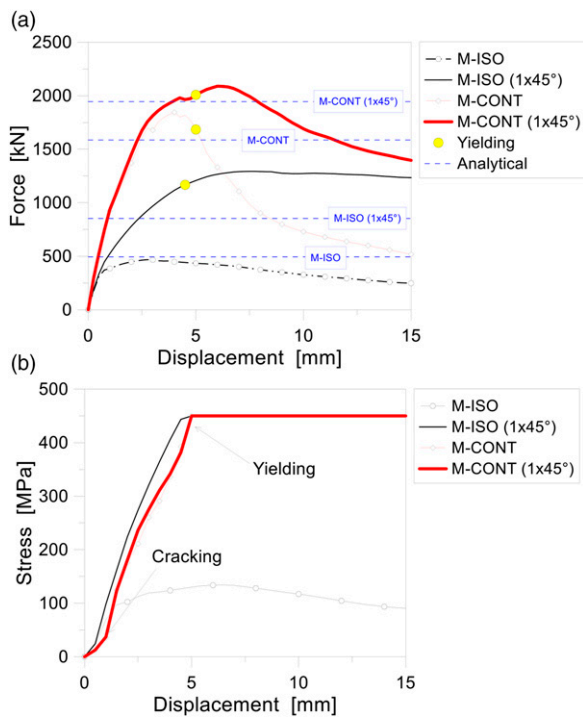
Figure 19. Load–displacement response of the full-scale RC slab in compression, with or without spirals and gap (ABAQUS): (a) load–displacement response and (b) stress evolution in the transverse rebar.

are optimally designed and placed to activate an enhanced resisting strut-and-tie mechanism as discussed in the Section Numerical analysis of a spiral-confined RC slab, minor cracks can be observed in the concrete components, with a mostly ductile overall response of the slab that takes the form of a more stable and regular load–displacement characteristic curve.

Analysis of a full-scale steel–concrete composite frame

Geometry

The selected steel–concrete composite frame takes inspiration from Figure 16 and with the experimental study originally discussed in Amadio et al. (2017b). The original structural system consists of two IPE300 type steel beams (2.1 m their nominal length), an HEB260 column (2.77 m the total height) and a solid RC slab (120 mm in thickness and 1.2 m in width). In the original investigation, moreover, steel shear studs (19 mm in diameter and 75 mm in total height) were used to provide a fully rigid mechanical connection between the slab and the steel beams. Those shear connectors were 75 mm and 150 mm spaced along the transverse and longitudinal beams axis, respectively.

In accordance with Section Analysis of a full-scale steel–concrete composite frame, the present study explores the RC slab under in-plane compression only, in order to evaluate the activation of resisting mechanisms and the possible benefit of additional spirals. Regarding its composition, material properties are considered as for f_{ck}= 35 MPa in the case of concrete (Figure 9) and f_y= 450 MPa for steel rebars. The longitudinal rebar are given by 8 ϕ 14 and 8 ϕ 6 bars, lying on the top and bottom layers of the slab, respectively. The primary transverse rebar consists of 5 ϕ 16 bars, 50 mm spaced, with a minimum distance of 220 mm from the column axis.

Numerical setup for confinement assessment

The RC slab and a short segment of the HEB260 column were extracted from the full FE assembly in Figure 16. The in-plane load-bearing capacity of the RC slab with or without steel spirals was thus explored according to Figure 17. More in detail, the HEB260 column was rigidly restrained towards possible displacements. The top face of the RC slab was subjected to a uniform imposed displacement uy, that was monotonically increased in the step time of analysis. At the same time, the longitudinal rebars were subjected to an equivalent imposed displacement u_y, as also schematized in Figure 17.

The same approach was considered for two limit conditions (both with or without steel spirals), herein detected as 'M-ISO' model (with isolated RC slab from the column and 'mechanism 2' only) and 'M-CONT' model, being representative of full ideal contact for the RC slab and the adjacent HEB260 column (with the effect of the activation of both mechanisms '1' and '2'). The schematic representation in Figure 16, as shown, is characterized by the presence of single spirals (45° their inclination) that realize the strut-and-tie mechanism on both the sides of the column. Different arrangements can be designed, in general, based on the available space and on the geometry of the composite system to verify.

Differing from the Section Analysis of a full-scale steel–concrete composite frame, variations in the reference FE model were represented by basic modifications in the geometrical features of the load-bearing components. Further, in terms of numerical modelling, the rigid 'tie' connection at the column-to-slab interface was replaced by a series of surface-to-surface contact interactions (0.3, the static friction coefficient). This choice was preferred to allow possible separation for the FE components in tension, and thus avoid potential stress peaks in the regions of interaction of the column with the slab. A total vertical displacement of 15 mm was imposed to the examined configurations.
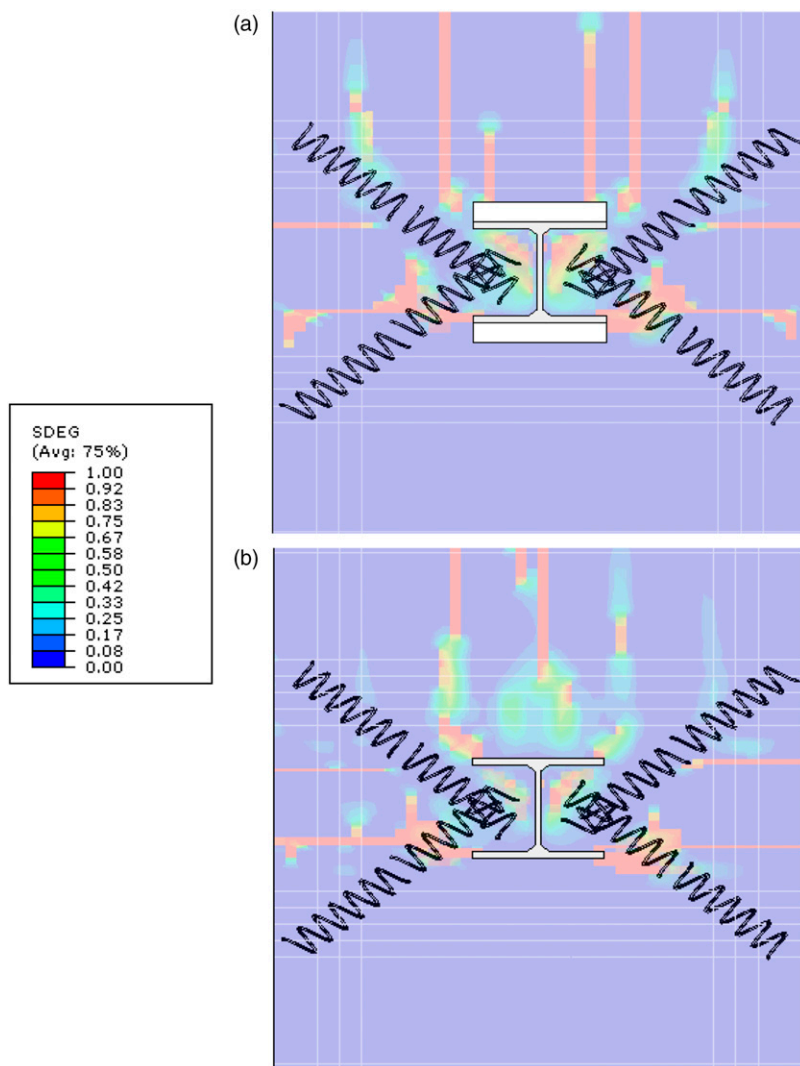
13

Figure 20. Concrete damage (SDEG) for the slab with steel spirals, as observed for the (a) M-ISO or (b) M-CONT configurations after 5 mm of deformation (ABAQUS; in evidence, 1/2th nominal geometry).

The column segment was then rigidly fixed at the lateral end sections, as schematized in Figure 17.

Load-bearing capacity

In order to assess and quantify the effect of steel spirals in the full-scale RC slab, the analysis of results was first focused on the total reaction force in each FE assembly. Given that the reference simulation consisted of a displacement-controlled analysis, this reaction force was calculated as the resultant vertical reaction transferred to the lateral (restrained) faces of the column.

The major outcome for the setup in Figure 17 takes the form of an improved strut-and-tie resisting mechanism that can be noticed in the vectorial stress distribution of Figure 18, for the M-ISO and M-CONT configurations,

respectively. The examples are selected at the achievement of ≈360 MPa in the transverse rebars, that is ≈0.8 times the actual yielding stress.

The typical load–displacement results can be found in Figure 19a. From the comparison of collected results, the first marked effect is represented by the presence of the gap or not in the slab. The 'M-ISO' and 'M-CONT' assemblies are thus characterized by severe variations in the total compressive resistance of the slab, as a direct effect of the corresponding mechanisms '1' and '2'. The M-CONT assembly, more in detail, is characterized by higher stiffness than the M-ISO, and much higher maximum resistance in compression. Besides, the same M-CONT model shows a slope variation in the load–displacement response, at a total displacement of ≈1.5 mm, that derives from the propagation of cracks in the

slab, with the consequent reduction of global stiffness and activation of the steel members. Once the RC slab is no more efficient due to severe damage, the residual resistance capacity of the M-CONT model decreases and is assigned to the transverse rebars only. In Figure 19a, analytical resistance values are also proposed for the examined configurations, as obtained from nominal material and geometrical properties in use.

Worth of interest in Figure 19a is the beneficial contribution that can be perceived especially for the proposed spirals in the M-ISO configuration. Besides, as expected, the M-CONT system takes minor benefit from the spirals introduction, in the initial stage of the collected load–displacement responses.

As shown for the M-ISO solution, the presence of spirals can be noticed in a certain increase of stiffness and resistance for the RC slab. This effect derives from the composite mechanism that the spirals can activate with the transverse rebars (once they are properly placed and designed).

In the case of the M-CONT assembly, the spirals are able to offer a limited post-cracked resistance and stiffness increase in the first 5 mm of imposed displacement, compared to the un-confined slab. Yielding of transverse rebars can be observed around $\approx$ 4–5 mm of deformation. Due to crushing of concrete, part of the spirals contribution vanishes for large imposed displacements but can be still noticed in comparison to the un-confined solution. On the other side, an optimal performance can be observed in Figure 19a for the M-ISO system with the confining spirals. The maximum resistance is calculated in the order of $\approx$500 kN for the un-confined system, and up to $\approx$2.5–3 times higher for the confined configuration. Most importantly, the confined M-ISO system suffers slightly for the concrete fracture. This effect can be appreciated in Figure 19a in the form of a rather stable overall trend for the load–displacement curve, with relevant post-cracked residual capacities.

Finally, it is worth to emphasize in Figure 19a that the residual resistance of both the un-confined M-ISO and M-CONT models tends to a comparable minimum value. Once the eventual contribution of concrete vanishes due to crushing, the final resistance and ductility of the system depends on the steel members only.

A more detailed analysis of the collected FE responses, in this regard, can be extended to the stress peaks in the transverse rebars, that are expected to take benefit and maximize their role from the strut-and-tie mechanism with the presence of spirals. Figure 19b, in this regard, shows the maximum stresses in the transverse rebars for all the examined configurations, as a function of the imposed displacement. It can be seen that steel members behave elastically up to $\approx$ 4–5 mm of deformation. Yielding appears more or less in the same order of displacement. This is not the case of the un-confined M-ISO system, where stress peaks are up to 150 MPa and the slab is not able to resist more.

Stress flow and damage

In conclusion, it is worth mentioning that the activation of a spiral-confined resisting mechanism for the slab is responsible of an overall improvement of the load-bearing performance of the involved components. In terms of stress distribution, the general trend and flows was already emphasized in Figure 18.

The observed fracture mechanism for both the configurations is found to agree with Figure 20. While concrete still cracks due to the imposed deformations and contact interactions in the region of the column, it can be noticed that the steel spirals ensure more stability and thus an improved stress redistribution in the global resisting mechanism.

Conclusions

The efficient design of steel–concrete composite frames and joints, as known, is a challenging issue which requires the definition and optimization of multiple parameters. In this regard, several literature studies proved to assess their seismic performance towards standard provisions and regulations. Compared to earlier studies, the attention was primarily focused on the use of spiral-based confinement technique to improve the overall resistance and ductility of the slab. More specifically, the in-plane compressive response of reinforced concrete slabs with steel spiral confinement was numerically explored. Such a confinement technique was proposed to address the possible activation of an improved resisting 'mechanism 2', in which the introduced spirals can enhance the basic strut-and-tie mechanism.

More in detail, the proposed intervention is based on the use of diagonal steel spirals, that are expected to enforce the resistance and ductility of the RC slab. The basic technique took inspiration from the use of spirals for the seismic improvement of RC members (especially columns), due to their positive confinement contribution.

Major advantage was taken from the finite element (FE) numerical analysis of validated models, with the support of literature experimental data for a small-scale slab prototype and a full-scale frame. The parametric analysis was carried out for several configurations of technical interest, including a focus on the local and global structural effects due to different arrangements for the proposed steel spirals (number, inclination). To this aim, the comparative analysis was carried out in terms of load-bearing capacity, as well as of stress flow evolution and damage propagation in the slab components.

As shown, these spirals can be considered as optimally placed once they actively contribute to carry on the stress peaks and modify the stress flow distribution in the slab components. In this condition, the parametric study proved that the strength of concrete struts can be efficiently increased, with marked benefits for the overall resisting mechanisms of the slab, and thus for the steel–composite frame as a whole. At the same time, the efficient contribution of spirals can be exploited in a certain ductility increase for the confined slab.

Declaration of conflicting interests

Funding

ORCID iD

Chiara Bedon ⓘ https://orcid.org/0000-0003-3875-2817

References

Alfarah B, López-Almansa F and Oller S (2017) New methodology for calculating damage variables evolution in Plastic Damage Model for RC structures. *Engineering Structures* 132: 70–86.

Amadio C, Pecce MR, Fasan M, et al. (2016) *Linee guida per la progettazione sismica di nodi composti acciaio-calcestruzzoResearch project RP3 of the ReLUIS-DPC 2014-2018*. ReLUIS.

Amadio C, Bedon C, Fasan M, et al. (2017a) Refined numerical modelling for the structural assessment of steel-concrete composite beam-to-column joints under seismic loads. *Engineering Structures* 138: 394–409.

Amadio C, Bedon C and Fasan M (2017b) Numerical assessment of slab-interaction effects on the behaviour of steel-concrete composite joints. *Journal of Constructional Steel Research* 139: 397–410.

Aribert J, Ciutina A and Dubin D (2006) *Seismic Response of Composite Structures Including Actual Behaviour of Beam-To-Column Joints*. Compos Constr Steel Concr, pp. 708–717.

Braconi A, Elamary A, Lucchesi D, et al. (2007) Improvement of seismic performance of steel-concrete composite joints by means of slab-column connections. In: Proceedings of ANIDIS Conference. June 10-14. Pisa, Italy.

CEN (2004) *Eurocode 8 - Design Provisions for Earthquake Resistance of Structures. Part 1.3: General Rules. Specific Rules for Various Materials and Elements*. Brussels, Belgium: CEN, European Committee for Standardization.

Li W, Li Q, Jiang W, et al. (2011) Seismic performance of composite reinforced concrete and steel moment frame structures – state-of-the-art. *Composites Part B: Engineering* 42(2): 190–206.

Marvel L, Doty N, Lindquist W, et al. (2014) Axial behavior of high-strength concrete confined with multiple spirals. *Engineering Structures* 60: 68–80.

Pecce M and Rossi F (2015) The experimental behavior and simple modeling of joints in composite MRFs. *[Eye Science Electronic Resource]* 105: 249–263.

Sankholkar PP, Pantelides CP and Hales TA (2018) Confinement Model for Concrete Columns Reinforced with GFRP Spirals. *Journal of Composites for Construction* 22: 3.

Simões R, Simões da Silva L and Cruz P (2001) Experimental behaviour of end-plate beam-to-column composite joints under monotonical loading. *[Eye Science Electronic Resource]* 23: 1383–1409.

Simões R and Simões da Silva L (2001) Cyclic behaviour of end-plate beam-to-column composite joints. *Steel Compos Struct* 1(3): 355–376.

Salvatore W, Bursi OS and Lucchesi D (2005) Design, testing and analysis of high ductile partial-strength steel–concrete composite beam-to-column joints. *Comput Struct* 83(28–30): 2334–2352.

Simulia (2020) *ABAQUS Computer Software*, RI, USA. Providence.

Tartaglia R, D'Aniello M, Rassati G, et al. (2018) Influence of composite slab on the nonlinear response of extended end-plate beam-to-column joints. *Key Engineering Materials* 10763: 4028818–4028825. www.scientific.net/KEM.763

Thermou GE, Elnashai AS, Plumier A, et al. (2004) Seismic design and performance of composite frames. *Chemical Society Reviews* 60: 31–57.